# A generalized multiplicative regularization for input estimation

Mathieu Aucejo, Olivier de Smet

# A generalized multiplicative regularization for input estimation

M. Aucejo[a], O. De Smet[a]

[a]*Laboratoire de Mécanique des Structures et des Systèmes Couplés, Conservatoire National des Arts et Métiers, 2 Rue Conté, 75003 Paris, France*

**Abstract**

This paper implements a generalized multiplicative regularization for estimating the mechanical loads acting on a linear structure. The proposed strategy extends the ordinary multiplicative regularization, previously published by the authors, by introducing an extra tuning parameter, which is determined through an original iterative procedure. To assess the practical interest and the overall performances of the proposed approach, numerical and real-world applications are proposed. Obtained results illustrate the influence of the extra tuning parameter according to the measurement noise level and highlight the benefits brought by the generalized multiplicative regularization in terms of solution accuracy.

*Keywords:* Linear inverse problem, Force reconstruction, Multiplicative regularization.

## 1. Introduction

Input estimation remains an important problem for the structural dynamics community as evidenced by the abundant literature dedicated to this

*Corresponding author. E-mail address: mathieu.aucejo@lecnam.net

topic in the recent years. Generally speaking, inverse methods can be classified into two groups. The first group includes methods that are specifically designed to solve the inverse problem in the time or frequency domains. In the time domain, one can cite Kalman-like approaches [1–3] or dynamic programming [4–6] , while, in the frequency domain, methods based on the filtering of the equation of motion of structures, such as beams, cylindrical shells or plates, have been developed [7–9] The second group gathers more general approaches that can be used indistinctly in both domains. This is, for instance, the case of methods based on the virtual work principle [10–12]. However, among all the methods belonging to this second group, regularization techniques are certainly the most widely used, because it allows including some prior information on the sources to identify. From a mathematical standpoint, the latter information is encoded in a regularization term generally incorporated in the formulation as an additive constraint to give rise to the so-called Tikhonov-like regularization [13]. Although this form of additive regularization has proved its efficiency to solve force reconstruction problems [14–16] , it requires the determination of the well-known regularization parameter. Unfortunately, this task reveals to be far from easy and automatic selection procedures have been developed for this purpose, such as the Generalized Cross-Validation [17], the L-curve principle [18] or the Bayesian indicator [19] to cite only only a few of them . However, it should be mentioned that all the above-cited selection techniques are generally computationally intensive and have been developed in the context of Tikhonov regularization (a.k.a. $\ell_2$-regularization). It results that they cannot be easily or directly applied to more general additive regularizations, such as $\ell_1$ [20],

$\ell_q$ [21] or mixed-norm regularizations [22]. To circumvent to this potential undesirable feature, we have recently introduced the ordinary multiplicative regularization in the context of structural source identification [23–25]. In its more general form, the proposed multiplicative regularization is expressed as:

$$\widehat{\mathbf{F}} = \underset{\mathbf{F}\setminus\{\mathbf{0}\}}{\operatorname{argmin}}\, \mathcal{F}(\mathbf{X}, \mathbf{F}) \cdot \mathcal{R}(\mathbf{F}), \tag{1}$$

where:

- $\mathbf{X}$ and $\mathbf{F}$ are the measured vibration field and the unknown excitation field respectively;
- $\mathcal{F}(\mathbf{X}, \mathbf{F})$ is the data-fidelity term, which is a measure of the deviation of the estimated vibration field from the measured one. It actually encodes prior information related to the noise corrupting the data [26];
- $\mathcal{R}(\mathbf{F})$ is the regularization term that encodes prior information on the excitation field $\mathbf{F}$ [27].

One of the remarkable properties of the previous formulation is that the corresponding solution is the point of intersection between the L-curve and a straight line with a slope equal to $-1$ [23]. In this regard, it can be interesting to add an extra tuning parameter that brings a greater flexibility by modifying the slope of the straight line and so the identified solution. Such an idea has been introduced by Regińska [28] and further developed by Viloche Bazán [29] in the context of Tikhonov regularization to only compute the corresponding optimal regularization parameter $\widehat{\alpha}$. In those papers, the

regularization parameter is sought such that:

$$\widehat{\alpha} = \underset{\alpha \in \mathbb{R}^{+*}}{\operatorname{argmin}} \, \mathcal{F}(\mathbf{X}, \mathbf{F}_\alpha) \cdot \mathcal{R}(\mathbf{F}_\alpha)^\mu, \tag{2}$$

where $\mathbf{F}_\alpha$ is the solution of the Tikhonov regularization for a given regularization parameter $\alpha$, while $\mu \in \mathbb{R}^{+*}$ is an extra tuning parameter. Practically, Eq. (2) is solved from a fixed-point algorithm that automatically adjusts the value of the extra tuning parameter [29].

In the light of these works, this paper proposes to revisit the ordinary multiplicative regularization by introducing an extra tuning parameter in the framework we have previously developed to efficiently solve input estimation problems. This particular form of multiplicative regularization, referred to as Generalized Multiplicative Regularization (GMR) in the rest of the paper, differs from the works of Regińska and Viloche Bazán by its philosophy, since it considers more general regularization terms and aims at solving the formulation as a whole. In particular, this means that the identified excitation field, the related regularization parameter and the extra tuning parameter are computed within the same iterative resolution procedure. Hence, the basic motivation of this paper is to assess the applicability of the GMR for identifying mechanical loads acting on a structure. To this end, the mathematical formulation of the GMR and the related resolution algorithm are detailed in section 2. In section 3, a numerical experiment is carried out to thoroughly analyze the influence of the extra tuning parameter on the identified solution according to the measurement noise level. Based on these results, an original iterative procedure is proposed in section 4 to automatically compute an optimal value of the extra tuning parameter. Finally, a real-world experiment is

carried out in section 5 to assess the ability of the whole resolution procedure in providing consistent reconstructions in operating conditions.

## 2. Generalized Multiplicative Regularization

This section introduces the mathematical formulation of the Generalized Multiplicative Regularization (GMR), as well as its resolution algorithm. More specifically, this section highlights the main features of the GMR and focuses on the basic steps of the resolution process.

### *2.1. General formulation*

As stated in the introduction, the GMR follows the idea proposed by Regińska and Viloche Bazán consisting in introducing an extra tuning parameter in the formulation of the functional to minimize. It results that the target excitation field $\widehat{\mathbf{F}}$ is sought as the solution of the following minimization problem:

$$\widehat{\mathbf{F}} = \underset{\mathbf{F}\setminus\{\mathbf{0}\}}{\operatorname{argmin}} \, \mathcal{F}(\mathbf{X}, \mathbf{F}) \cdot \mathcal{R}(\mathbf{F})^{\mu}. \tag{3}$$

To explicitly define the data fidelity and regularization terms, $\mathcal{F}(\mathbf{X}, \mathbf{F})$ and $\mathcal{R}(\mathbf{F})$, three assumptions are made. The first one consists in considering the studied structures as linear and time-invariant systems. If we further assume that the mechanical problem is expressed in the frequency domain, then the dynamic behavior of the structure is completely determined by the transfer functions matrix $\mathbf{H}$, relating the vibration field $\mathbf{X}$ to the excitation field $\mathbf{F}$, such that:

$$\mathbf{X} = \mathbf{H}\mathbf{F} + \mathbf{N}, \tag{4}$$

where $\mathbf{N}$ models the noise corrupting the measured data.

The second assumption is related to the statistical properties of the noise vector previously defined. Indeed, it has been recalled in the very beginning of this paper that the data-fidelity encodes any prior information available on the measurement noise. In this respect, the data-fidelity term has to reflect the main characteristics of the actual noise. Consequently, if the noise is supposed Gaussian and spatially white, the data-fidelity term is expressed as [30, 31]:

$$\mathcal{F}(\mathbf{X}, \mathbf{F}) = \|\mathbf{X} - \mathbf{H}\mathbf{F}\|_2^2. \tag{5}$$

The last assumption concerns the definition of the regularization term, which encodes one's prior knowledge of the spatial distribution of the excitation sources over the structure. Generally, forces of different nature can act simultaneously on a structure. As a result, it is supposed that the structure is excited in $R$ different regions by local excitation fields $\mathbf{F_r}$ of various types (localized or distributed, for instance). Formally, this naturally leads to introduced local regularization terms $\mathcal{R}(\mathbf{F_r})$, which are defined such that:

$$\mathcal{R}(\mathbf{F_r}) = \|\mathbf{F_r}\|_{q_r}^{q_r}, \tag{6}$$

where $\| \bullet \|_{q_r}$ is the $\ell_{q_r}$-norm (or quasi-norm), while $q_r$ is the related norm parameter defined in $\mathbb{R}^{+*}$. The latter parameter allows promoting either a sparse (or localized) excitation field when $q_r \leq 1$ or a smooth (or distributed)

one when $q_r \geq 2$[1].

Formally, the local regularization terms can be combined in an additive or a multiplicative manner [25]. The one retained in this paper is based on a Bayesian analysis and consists in defining the regularization term as the sum of the local regularization terms, that is:

$$\mathcal{R}(\mathbf{F}) = \sum_{r=1}^{R} \|\mathbf{F_r}\|_{q_r}^{q_r}. \tag{7}$$

By bringing everything together, the general form of the GMR considered in this paper is finally written:

$$\widehat{\mathbf{F}} = \underset{\mathbf{F}\setminus\{\mathbf{0}\}}{\operatorname{argmin}} \|\mathbf{X} - \mathbf{HF}\|_2^2 \cdot \left( \sum_{r=1}^{R} \|\mathbf{F_r}\|_{q_r}^{q_r} \right)^{\mu}. \tag{8}$$

At this stage, two comments can be made regarding the global behavior of the GMR. First of all, whatever the particular form of the data-fidelity and regularization terms, the solution obtained from the GMR is the point at which the corresponding L-curve is tangent to a straight line having a slope equal to $-1/\mu$. A general proof of this statement can be found in Ref. [28]. Then, the solution obtained from the GMR is directly conditioned to the value of the extra tuning parameter $\mu$. Indeed, when $\mu = 0$, the GMR reduces to an Ordinary Least Squares regression, whereas it reduces to the Ordinary Multiplicative Regularization (OMR) when $\mu = 1$ [23, 25]. More generally, solutions minimizing the data-fidelity term are promoted when $\mu < 1$, while solutions minimizing the regularization term are favored when $\mu > 1$. To

[1]In the present paper, the subscript $r$ (bold or italic) refers to a particular region of the structure. From a notation point of view, a bold character ($\mathbf{r}$) is used for vectors and matrices, while an italic character ($r$) is used for scalar quantities.

some extent, $\mu$ can be seen as a trade-off parameter, since it allows weighting the relative importance of the data-fidelity and regularization terms.

### *2.2. Resolution algorithm*

The resolution of the GMR requires the implementation of an iterative procedure. From a very general standpoint, the resolution algorithm is divided into three main steps:

1. set $k = 0$ and initialize $\widehat{\mathbf{F}}^{(0)}$
2. **while** convergence is not reached **do**
   a. Compute $\widehat{\mathbf{F}}^{(k+1)}$
   b. Compute the convergence indicator

   **end while**
3. **return** $\widehat{\mathbf{F}}$

In the present paper, the initialization step as well as convergence monitoring are not described and the interested reader can refer to Ref. [23] for further information. Actually, the core of the proposed algorithm is the computation of the excitation field at iteration $k+1$ (step 2.a), around which all the procedure is built. Practically, it is derived from the direct application of the first-order optimality condition to the functional:

$$J(\mathbf{F}) = \|\mathbf{X} - \mathbf{H}\mathbf{F}\|_2^2 \cdot \left( \sum_{r=1}^{R} \|\mathbf{F}_\mathbf{r}\|_{q_r}^{q_r} \right)^{\mu}. \tag{9}$$

In doing so, the fixed-point iterate at iteration $k+1$ is written:

$$\widehat{\mathbf{F}}^{(k+1)} = \left( \mathbf{H}^H \mathbf{H} + \alpha^{(k+1)}\, \mathbf{W}^{(k+1)} \right)^{-1} \mathbf{H}^H \mathbf{X}, \tag{10}$$

where $\alpha^{(k+1)}$ is the adaptive regularization parameter, while $\mathbf{W}^{(k+1)}$ is a global weighting matrix. Formally, the adaptive regularization parameter $\alpha^{(k+1)}$ is defined by the relation:

$$\alpha^{(k+1)} = \mu \frac{\left\| \mathbf{X} - \mathbf{H}\widehat{\mathbf{F}}^{(k)} \right\|_2^2}{\sum_{r=1}^{R} \left\| \widehat{\mathbf{F}}_{\mathbf{r}}^{(k)} \right\|_{q_r}^{q_r}}. \tag{11}$$

On the other hand, the global weighting matrix $\mathbf{W}^{(k+1)}$ is defined such that:

$$\mathbf{W}^{(k+1)} = \text{diag}\left[ \mathbf{W}_{\mathbf{1}}^{(k+1)}, \ldots, \mathbf{W}_{\mathbf{r}}^{(k+1)}, \ldots, \mathbf{W}_{\mathbf{R}}^{(k+1)} \right]. \tag{12}$$

In the previous relation, each local weighting matrix $\mathbf{W}_{\mathbf{r}}^{(k+1)}$ is a diagonal matrix given by:

$$\mathbf{W}_{\mathbf{r}}^{(k+1)} = \text{diag}\left[ w_{r,1}^{(k+1)}, \ldots, w_{r,i}^{(k+1)}, \ldots, w_{r,N_r}^{(k+1)} \right] \tag{13}$$

with

$$w_{r,i}^{(k+1)} = \frac{q_r}{2} \max\left( \epsilon_r, \left| \widehat{F}_{ri}^{(k)} \right| \right)^{q_r - 2}, \tag{14}$$

where $N_r$ is the number of identification point in the region $r$, $\widehat{F}_{ri}^{(k)}$ is the i$^{\text{th}}$ component of the local excitation vector $\widehat{\mathbf{F}}_{\mathbf{r}}^{(k)}$, while $\epsilon_r$ is a small positive number avoiding infinite weights when $\left| \widehat{F}_{ri}^{(k)} \right| \to 0$ and $q_r < 2$. The value of this parameter is chosen so that 5% of the values of $\left| \widehat{\mathbf{F}}^{(0)} \right|$ are less than or equal to $\epsilon_r$ [21].

## 3. Numerical experiment

The numerical experiment proposed in this section aims at analyzing the behavior and the performances of the GMR on an academic application.

More specifically, the main objective of this application is twofold. First, it is intended to assess the influence of the extra tuning parameter $\mu$ on the solutions identified by the GMR. Second, it is sought to determine whether an overall trend emerges from the simulation results regarding the evolution of $\mu$ with respect to the measurement noise level.

### *3.1. Test case description*

The present numerical experiment aims at identifying a unit point force exciting, at 350 Hz, a simply-supported steel plate as well as the resulting reaction forces at boundaries. The dimensions of the plate are 0.6 m $\times$ 0.4 m $\times$ 0.005 m while the external point force is located at point $(x_0, y_0) = (0.42 \text{ m}, 0.25 \text{ m})$, measured form the lower left corner of the plate.

To carried out this numerical experiment, a synthesized vibration field and the transfer functions matrix of the structure must be provided as input data to the GMR. The generation of the experimental data is performed in two steps. First, the noiseless reference displacement field $\mathbf{X_{ref}}$ is computed from a FE mesh of the plate made up with 187 shell elements[2], assuming that only bending motions are measured. Then, a Gaussian white noise with a prescribed signal-to-noise Ratio (SNR) is added to the reference data to simulate the measured vibration field. As for the definition of the transfer function matrix $\mathbf{H}$, it has been chosen to compute it from the FE model of the plate with free boundary conditions, assuming, here again, that only bending motions are measurable. Such a modeling enables the reconstruction

[2]The FE mesh has been defined using 8 elements per bending wavelength. Consequently, the current mesh is theoretically valid up to 590 Hz.

of the point force and the reaction forces, insofar as they are then considered external to the system.

Finally, it is necessary to define the reference force vector $\mathbf{F_{ref}}$, that could serve as a benchmark, as well as a set of qualitative indicators measuring the accuracy of the identified solutions. In the present case, the reference force vector must include the external point force as well as the reaction forces at boundaries, since their reconstruction is the primary objective of the proposed numerical experiment. This is for this particular reason that the reference force vector is computed as follows:

$$\mathbf{F_{ref}} = \mathbf{H}^{-1}\mathbf{X_{ref}}. \tag{15}$$

Fig. 1 presents the spatial distribution of the sources to identify. As expected from the problem description, the reference force vector exhibits smooth reaction forces at boundaries of the plate as well as a unit point force $F_0$ at $(x_0, y_0) = (0.42 \text{ m}, 0.25 \text{ m})$.

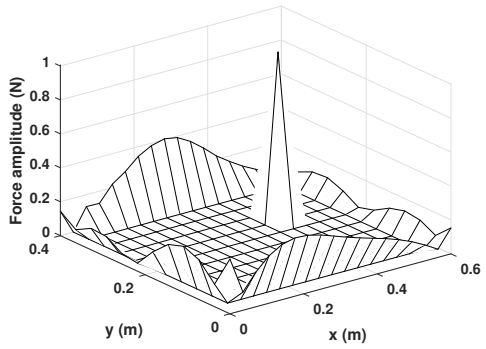


Figure 1: Reference force vector $\mathbf{F_{ref}}$ at 350 Hz

Regarding the definition of qualitative indicators allowing to assess the

actual performances of the GMR, three particulars indicators have been implemented: the global relative error (GRE), the relative error on the identification of the reaction forces (RERF) and the peak error (PE). Formally, the global relative error is a global indicator of the reconstruction quality, defined by the relation:

$$\mathrm{GRE} = \frac{\left\| \widehat{\mathbf{F}} - \mathbf{F}_{\mathbf{ref}} \right\|_1}{\|\mathbf{F}_{\mathbf{ref}}\|_1}. \tag{16}$$

In a similar fashion, the relative error on the reaction forces is an indicator of the reconstruction quality of the reaction forces. Its mathematical definition is similar to the global relative error, since:

$$\mathrm{RERF} = \frac{\left\| \widehat{\mathbf{F}}^{(\mathrm{rf})} - \mathbf{F}^{(\mathrm{rf})}_{\mathbf{ref}} \right\|_1}{\left\| \mathbf{F}^{(\mathrm{rf})}_{\mathbf{ref}} \right\|_1}, \tag{17}$$

where $\widehat{\mathbf{F}}^{(\mathrm{rf})}$ is the force vector corresponding to the identified reaction forces at boundaries , while $\mathbf{F}^{(\mathrm{rf})}_{\mathbf{ref}}$ is the related reference force vector.

Contrary to the foregoing indicators, the peak error is a local indicator describing the reconstruction quality of the point force amplitude. Mathematically, it is defined such that:

$$\mathrm{PE} = \frac{\widehat{F}_p - F_p^{\mathrm{ref}}}{F_p^{\mathrm{ref}}}, \tag{18}$$

where $F_p^{\mathrm{ref}}$ is the point force amplitude associated to the reference force vector $\mathbf{F}_{\mathbf{ref}}$, while $\widehat{F}_p$ is the point force amplitude associated to the identified solution $\widehat{\mathbf{F}}$ at point $(x_0, y_0)$.

Finally, it worth mentioning that the quality of the identified excitation field is conditioned to the convergence of FE mesh used to build the the transfer functions matrix. Indeed, at a particular frequency, the FE model must

be fine enough to properly describe the dynamic behavior of the structure, which is the case here. Another possibility, not used in this work, consists in computing the transfer functions matrix for a converged mesh and then applying selection matrices to fit with the measurement and reconstruction meshes.

### *3.2. Application*

In this section, the behavior and the performances of the GMR with respect to the value of the extra tuning parameter $\mu$ and the measurement noise level are investigated. More precisely, by applying the GMR for various SNR values ranging from 30 dB to 0 dB (i.e. from weakly to extremely noisy data), one expects to see a trend emerge for the parameter $\mu$ with the measurement noise level. But before that, it remains to characterize the identification regions as well as the value of the related norm parameters $q_r$. Following the description of the problem and the distribution of the sources presented in Fig. 1, two identification regions can be defined: (i) a central region associated to the norm parameter $q_1$ and including the external point force only and (ii) a region corresponding to the boundaries of the plate and associated to the norm parameter $q_2$ [see Fig. 2]. Practically, this division invites us to promote the sparsity of the excitation field in the central region and its continuity at boundaries. From the indications given in section 2.1 and our own experience of such problems [31], choosing $q_1 = 0.5$ and $q_2 = 2$ fulfills this requirement.

To properly analyze the influence of $\mu$ on the reconstruction accuracy, the results obtained from the Ordinary Multiplicative Regularization (OMR), corresponding to the GMR for $\mu = 1$, are first presented in Table 1 and Fig. 3

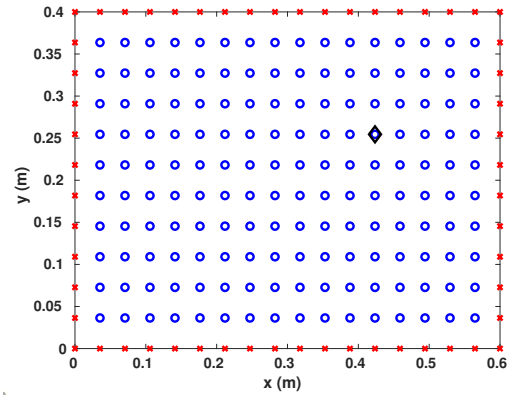


Figure 2: Definition of the identification regions - ($\circ$) region 1 (Point force), ($\times$) region 2 (Reaction forces) and ($\Diamond$) location of the point force

for the sake of comparison. In the present case, the OMR globally leads to satisfying reconstructions both qualitatively and quantitatively, except for extremely low SNR value (i.e. 0 dB), for which the point force is not identified contrary to the reaction forces. For the sake of the completeness, the reconstructions obtained for $\mu = 0.5$ and $\mu = 2$ are presented in Appendix A.

Practically, better solutions may be obtained by varying the value of the parameter $\mu$. Here, the parameter leading to an optimal solution is said itself optimal for the problem considered and is noted $\widehat{\mu}$ in the following. After a manual tuning, the optimal values of the extra parameter as well as the quality indicators are summarized in Table 2, while the corresponding excitation fields are presented in Fig. 4. Obtained results clearly emphasize the influence of the extra tuning parameter on the quality of the identified solutions. Indeed, whatever the SNR considered, it is possible to find a value of $\mu$ adapted to the problem and leading to a fair compromise between the

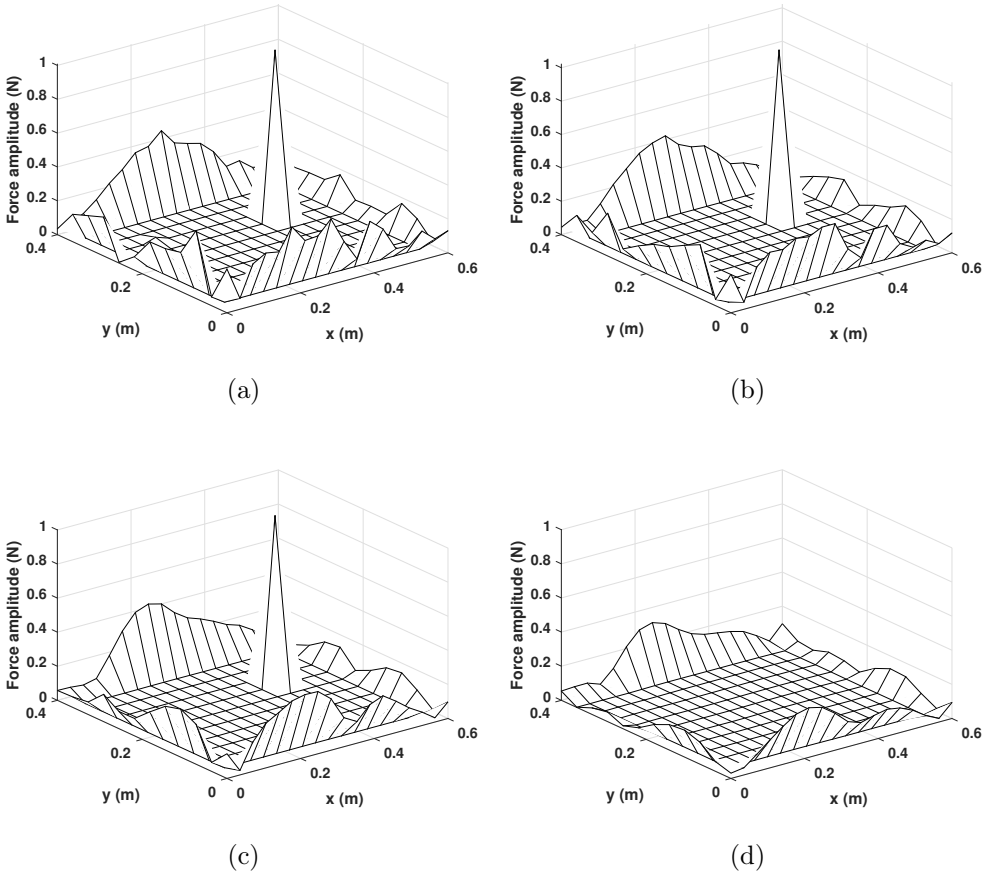


Figure 3: Reconstructed excitation field at 350 Hz from the OMR (i.e. GMR for $\mu = 1$) – (a) SNR = 30 dB, (b) SNR = 20 dB, (c) SNR = 10 dB and (d) SNR = 0 dB

Table 1: Performances of the OMR (GMR for $\mu = 1$) for various measurement noise levels – $N_{it}$: Number of iterations of the resolution algorithm

| | **SNR** | | | |
|---|---|---|---|---|
| **Indicators** | **30 dB** | **20 dB** | **10 dB** | **0 dB** |
| GRE (%) | 33.61 | 30.27 | 30.74 | 52.88 |
| RERF (%) | 35.79 | 31.81 | 31.10 | 45.52 |
| PE (%) | 0.83 | 2.25 | 0.16 | –99.45 |
| $N_{it}$ | 27 | 13 | 15 | 16 |

reconstruction of the point force and that of the reaction forces. This is especially noticeable for extremely noisy data (i.e. SNR = 0 dB). In this case, the point force location is identified at $(\widehat{x}_0, \widehat{y}_0) = (0.46 \text{ m}, 0.25 \text{ m})$ instead of $(x_0, y_0) = (0.42 \text{ m}, 0.25 \text{ m})$, corresponding to a location error less than 10%. On the other hand, the PE computed from the point force amplitude identified at $(\widehat{x}_0, \widehat{y}_0)$ is equal to 0.973 N instead of 1 N (see Table 2). Consequently, all things considered, this is a remarkable result for such an extreme configuration. Finally, it is worth noting that the optimal value of the extra tuning parameter decreases as the measurement noise level increases. More specifically, $\mu$ should be greater than 1 in case of weakly and moderately noisy data, while it should be less than or equal to 1 for highly and extremely noisy data. This observation perfectly reflects the subtle balance induced by the regularization process, i.e. the relative weighting of the data-fidelity and regularization terms controlled by the adaptive regularization parameter $\alpha$.

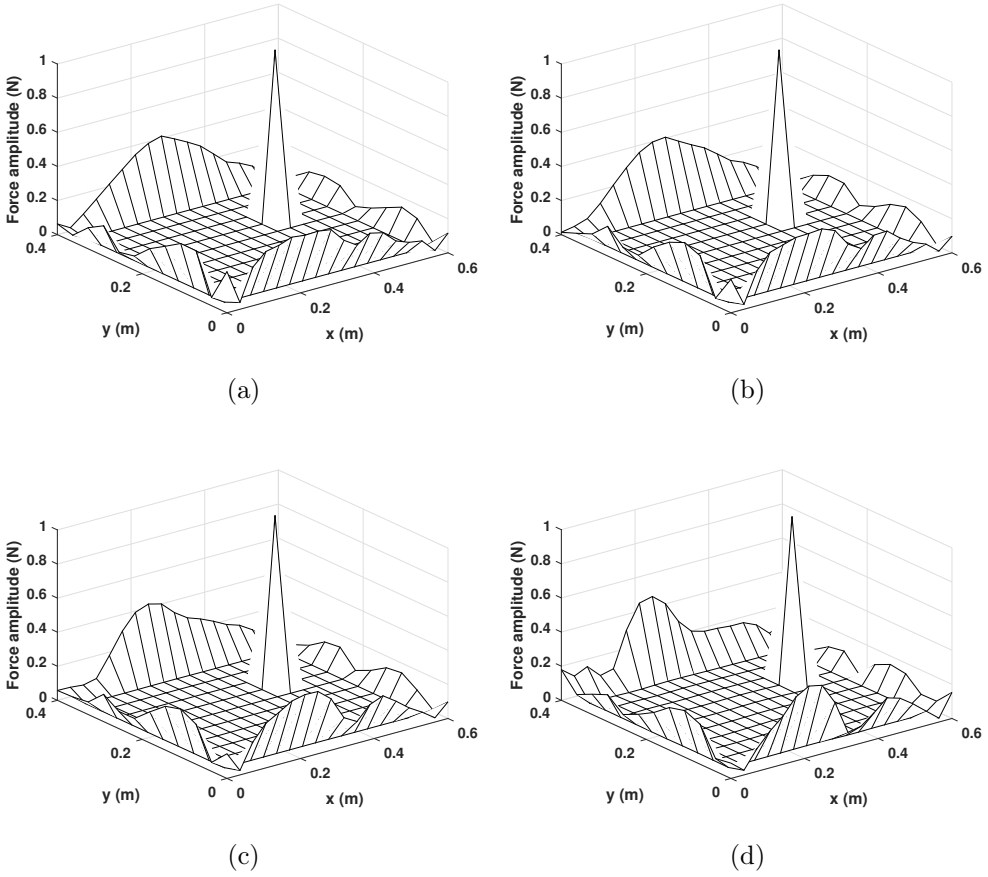


Figure 4: Reconstructed excitation field at 350 Hz from the GMR for $\mu = \widehat{\mu}$ (manually tuned) – (a) SNR = 30 dB, (b) SNR = 20 dB, (c) SNR = 10 dB and (d) SNR = 0 dB

Table 2: Performances of the GMR for the optimal parameter $\widehat{\mu}$ (manually tuned) for various measurement noise levels – $N_{it}$: Number of iterations of the algorithm

| | **SNR** | | | |
|---|---|---|---|---|
| **Indicators** | **30 dB** | **20 dB** | **10 dB** | **0 dB** |
| $\widehat{\mu}$ | 5 | 2.35 | 1 | 0.4 |
| GRE (%) | 15.10 | 20.04 | 30.74 | 71.39 |
| RERF (%) | 15.44 | 20.63 | 31.10 | 51.97 |
| PE (%) | $3.3\times10^{-3}$ | $4.2\times10^{-3}$ | 0.16 | –2.70 (*) |
| $N_{it}$ | 12 | 13 | 15 | 51 |

(∗) PE computed from the amplitude at the identified point force location

## 4. Automatic computation of the extra tuning parameter

The results obtained in the previous section have shown that the optimal value of the extra tuning parameter decreases with the SNR. However, finding this value a priori is far from an easy task. This observation points out the need for implementing an automatic selection procedure. In this section, an original fixed-point algorithm is introduced for this purpose.

### *4.1. Basic principle*

A careful analysis of the resolution algorithm, described in section 2.2, shows that an optimal solution should be obtained provided that [see Eq. (11)]:

$$\widehat{\alpha}\,\frac{\displaystyle\sum_{r=1}^{R}\left\|\widehat{\mathbf{F}}_{\mathbf{r}}\right\|_{q_r}^{q_r}}{\left\|\mathbf{X}-\mathbf{H}\widehat{\mathbf{F}}\right\|_2^2}\approx\mu, \tag{19}$$

where $\widehat{\alpha}$ is the value of the adaptive regularization parameter obtained at convergence of the resolution algorithm.

This observation suggests the definition of the following function:

$$\psi(\alpha,\mu) = \alpha \, \frac{\displaystyle\sum_{r=1}^{R} \|\mathbf{F}_{\mathbf{r}\alpha}\|_{q_r}^{q_r}}{\|\mathbf{X} - \mathbf{H}\mathbf{F}_{\alpha}\|_2^2}, \tag{20}$$

where $\mathbf{F}_{\alpha}$ is the solution of the additive counterpart of the GMR obtained for a constant regularization parameter $\alpha$, that is[3]:

$$\mathbf{F}_{\alpha} = \underset{\mathbf{F}}{\operatorname{argmin}} \, \|\mathbf{X} - \mathbf{H}\mathbf{F}\|_2^2 + \alpha \left( \sum_{r=1}^{R} \|\mathbf{F}_{\mathbf{r}}\|_q^q \right)^{\mu}, \tag{21}$$

while $\mathbf{F}_{\mathbf{r}\alpha}$ is the subset of $\mathbf{F}_{\alpha}$ restricted to the region $r$.

It results from Eqs. (19) and (20) that an optimal value of the extra regularization parameter $\widehat{\mu}$ should be found when:

$$\widehat{\mu} = \psi\left(\widehat{\alpha}, \widehat{\mu}\right), \tag{22}$$

which is equivalent to seek the solution such that $\widehat{\mathbf{F}} = \mathbf{F}_{\widehat{\alpha}}$.
This very basic observation suggests the implementation of the iterative algorithm presented in the next section and satisfying Eq. (22) within some tolerance when the iterative process has converged.

[3] $\mathbf{F}_{\alpha}$ is computed from the algorithm presented in section 2.2. However, the actual regularization parameter at iteration $k+1$ is $\alpha^{(k+1)} = \mu\,\alpha \left( \sum_{r=1}^{R} \left\| \mathbf{F}_{\mathbf{r}\alpha}^{(k)} \right\|_{q_r}^{q_r} \right)^{\mu-1}$ and not simply $\alpha$.

*4.2. Practical implementation*

Before detailing the practical implementation of the proposed iterative procedure, it is important to fully understand its expected behavior. To this end, let us take another look at the numerical experiment presented in section 3 for an SNR of 30 dB. The starting point of our reflection is illustrated in Fig. 5 presenting the plot of $\psi\left(\alpha, \mu_0\right)$ for $\mu_0 = 1$ ($\mu_0$: initial choice of the extra tuning parameter). This figure shows that the point $(\widehat{\alpha}_0, \mu_0)$, indicated by the marker $(*)$, does not lie on the curve defined by $\psi(\alpha, \mu_0)$, meaning that the corresponding initial solution $(\widehat{\mathbf{F}}_0, \widehat{\alpha}_0)$ is not optimal in the sense of Eq. (22).

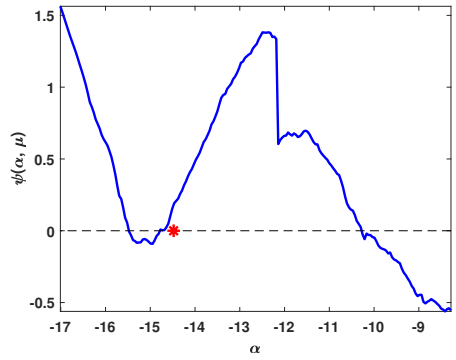


Figure 5: Plot of $\psi(\alpha, \mu_0)$ for $\mu_0 = 1$ – (—) $\psi\left(\alpha, \mu_0\right)$, $(--)$ $\mu = \mu_0$ and $(*)$ $\widehat{\alpha}_0$ (the abscissa and the ordinate are scaled logarithmically using the common logarithm)

For finding a value of $\mu$ adapted to the problem, it is chosen to apply the GMR once again using an updated value of $\mu$, noted $\mu_1$ and chosen such that $\mu_1 = \psi\left(\widehat{\alpha}_0, \mu_0\right)$ (see Fig. 6a). In doing so, the new point $(\widehat{\alpha}_1, \mu_1)$, associated to the updated solution $(\widehat{\mathbf{F}}_1, \widehat{\alpha}_1)$, is almost located on the curve defined by $\psi(\alpha, \mu_1)$ (see Fig. 6b), meaning that $\widehat{\mathbf{F}}_1 \approx \mathbf{F}_{\widehat{\alpha}_1}$, i.e. $\mu_1 \approx \psi(\widehat{\alpha}_1, \mu_1)$. Following

this first iteration, the process can be continued until the relative variation of $\mu$ between two successive iterations is less than or equal to some tolerance fixed by the user. The whole fixed-point algorithm used to determine the optimal triplet $(\widehat{\mathbf{F}}, \widehat{\alpha}, \widehat{\mu})$ is summarized by the pseudo-code presented in Algorithm 1.

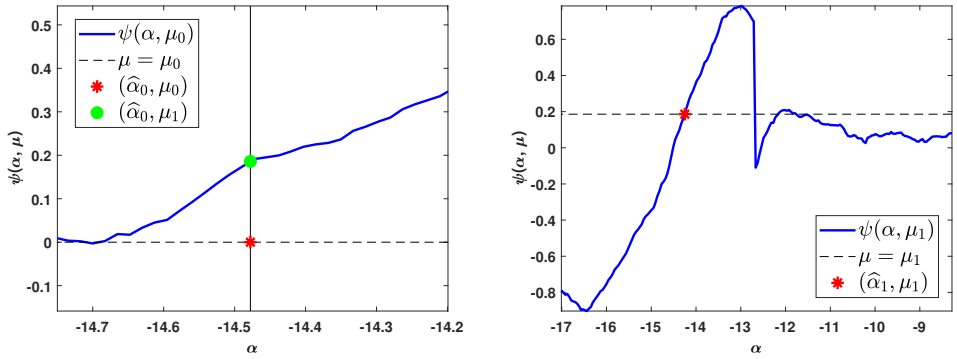


(a) (b)

Figure 6: Illustration of the first iteration of the process – (a) Selection of $\mu_1$ - zoomed portion of $\psi(\alpha, \mu_0)$ and (b) plot of $\psi(\alpha, \mu_1)$ (the abscissa and the ordinate are scaled logarithmically using the common logarithm)

### *4.3. Application*

For the numerical experiment considered in section 3, the application of the algorithm previously described for a tolerance set to $10^{-3}$ (i.e. 0.1%) allows obtaining the results gathered in Table 3 and Fig. 7. From the analysis of these results, some comments can be made. First of all, the value of the optimal extra tuning parameter found by the algorithm tends to decrease as the measurement noise level increases. This observation is actually in line with the conclusion drawn in section 3. Then, the value of $\mu$, retained by

**Algorithm 1:** Pseudo-code of the proposed iterative algorithm

**Inputs** : $\mathbf{X}$, $\mathbf{H}$, $q_r$, $tol$

**Outputs:** $\widehat{\mathbf{F}}$, $\widehat{\alpha}$, $\widehat{\mu}$

Set $j = 0$, $\delta = 1$, $\mu_0 = 1$

Compute $(\widehat{\mathbf{F}}_0, \widehat{\alpha}_0)$ from the GMR for $\mu_0$ (see section 2.2)

**while** $\delta > tol$ **do**

$\mu_{j+1} = \psi(\widehat{\alpha}_j, \mu_j)$

Compute $(\widehat{\mathbf{F}}_{j+1}, \widehat{\alpha}_{j+1})$ from the GMR for $\mu_{j+1}$

$\delta = \frac{|\mu_{j+1} - \mu_j|}{\mu_j}$

$j = j + 1$

**end**

$\widehat{\mathbf{F}} = \widehat{\mathbf{F}}_j$, $\widehat{\alpha} = \widehat{\alpha}_j$, $\widehat{\mu} = \mu_j$

the algorithm, leads to a reasonable compromise between the reconstruction accuracy of the point force and that of the reaction forces. Obviously, better solutions can be obtained by manually tuning $\mu$ (see section 3), but this is a perilous undertaking without a precise knowledge of the target excitation field. Finally, it should be noted that, for the two lowest SNR values (i.e. 10 dB and 0 dB), the proposed algorithm either has difficulty converging or even diverges due to numerical issues during the process.

However, in the light of the previous results and those presented in Fig. 6, it is legitimate to question the interest of continuing the iterative process beyond the first iteration in terms of solution accuracy and computational efficiency. To address this issue, the results obtained after the first iteration of the algorithm are given in Table 4 and Fig. 8. It can be especially noted

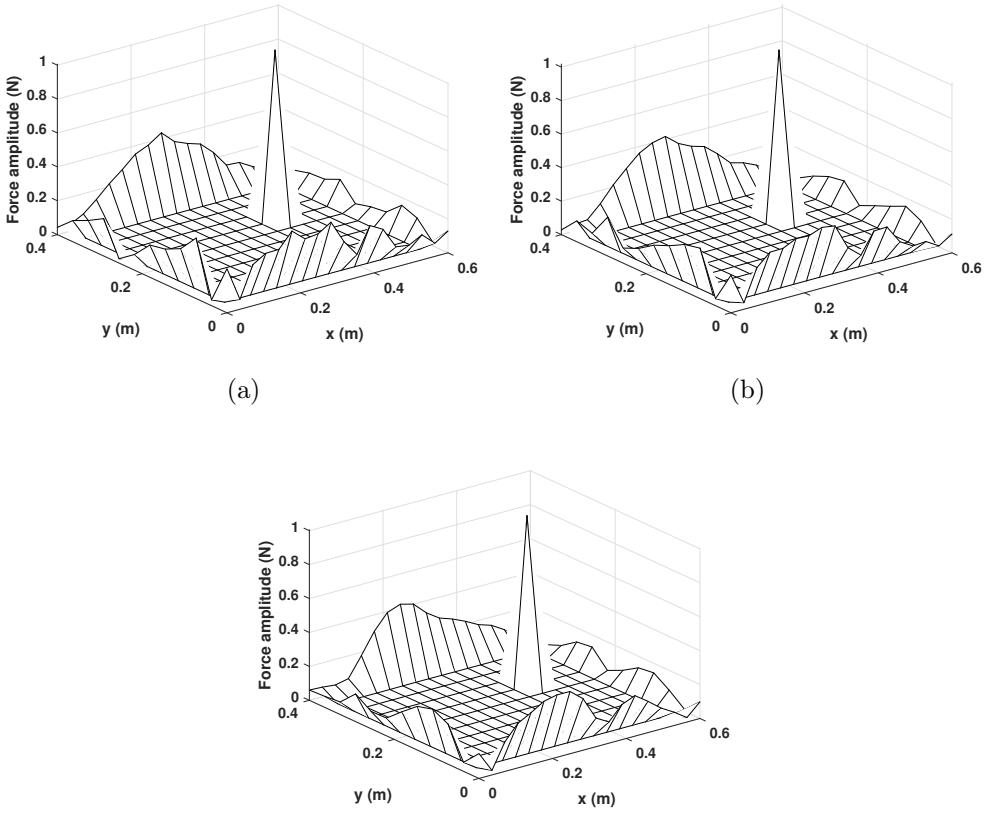


(a)




(b)




(c)

Figure 7: Reconstructed excitation field at 350 Hz from the GMR for $\mu = \widehat{\mu}$ – (a) SNR = 30 dB, (b) SNR = 20 dB and (c) SNR = 10 dB

Table 3: Performances of the GMR for $\mu = \widehat{\mu}$ for various measurement noise levels – $N_{it}$: Number of iterations of the algorithm

| | **SNR** | | | |
|---|---|---|---|---|
| **Indicators** | **30 dB** | **20 dB** | **10 dB** | **0 dB** |
| $\widehat{\mu}$ | 1.57 | 1.23 | 0.96 | – |
| GRE (%) | 26.06 | 26.95 | 31.21 | – |
| RERF (%) | 27.79 | 28.24 | 31.57 | – |
| PE (%) | 0.69 | 1.86 | 0.60 | – |
| $N_{it}$ | 4 | 6 | 200 $(*)$ | – |

$(*)$ Maximum number of iterations allowed for the main loop

that the quality of the reconstructed excitation field is not significantly improved by completing the iterative process. Perhaps more interesting is the result obtained in case of extremely noisy data (i.e. SNR = 0 dB). Indeed, contrary to what observed previously, a solution is obtained by stopping the process right after its first iteration. As observed in section 3.2, the point force location is not properly identified (see PE in Table 4), while the reaction forces are reasonably well estimated. A closer look at Fig. 8d shows that the reconstructed point force is actually located at $(\widehat{x}_0, \widehat{y}_0) = (0.46 \text{ m}, 0.25 \text{ m})$ with an amplitude of 0.84 N. Quantitatively, this corresponds to a PE equals to –15.4% for a location error less than 10%, which remains acceptable considering such a low SNR.

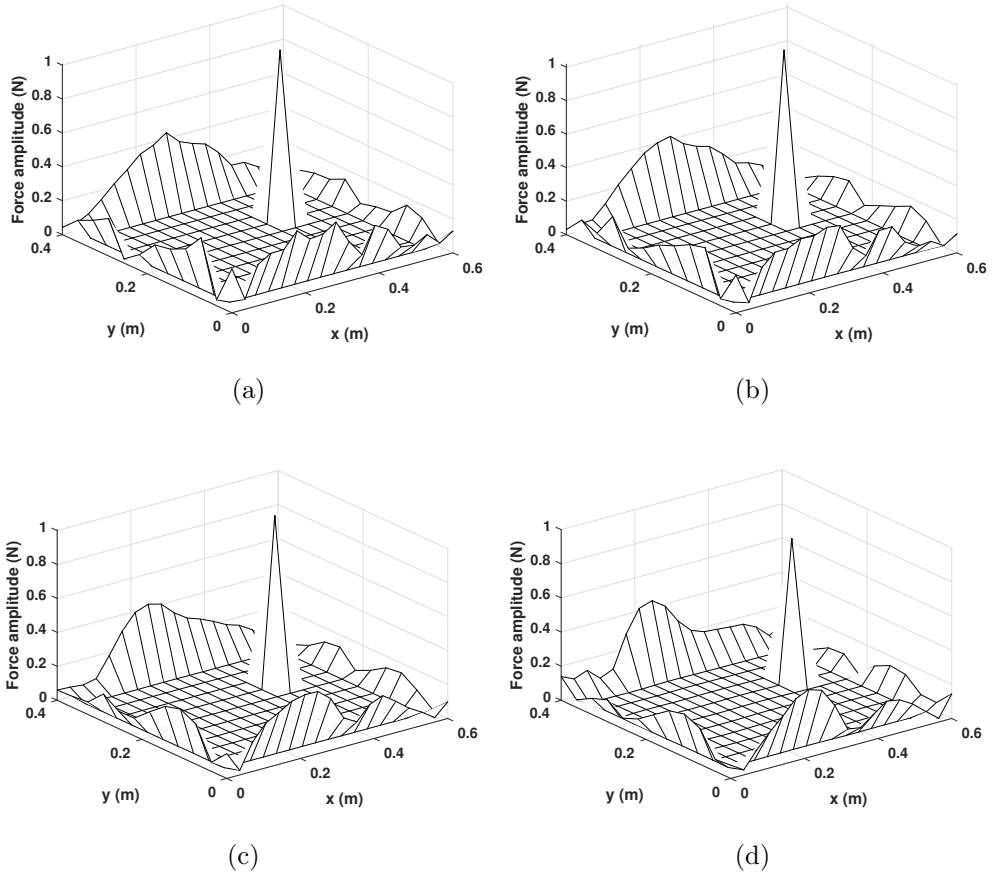


Figure 8: Reconstructed excitation field at 350 Hz from the GMR for $\mu = \mu_1$ – (a) SNR = 30 dB, (b) SNR = 20 dB, (c) SNR = 10 dB and (d) SNR = 0 dB

Table 4: Performances of the GMR for $\mu = \mu_1$ for various measurement noise levels

| | **SNR** | | | |
|---|---|---|---|---|
| **Indicators** | **30 dB** | **20 dB** | **10 dB** | **0 dB** |
| $\mu_1$ | 1.53 | 1.19 | 0.97 | 0.50 |
| GRE (%) | 26.37 | 27.42 | 31.16 | 63.69 |
| RERF (%) | 28.15 | 28.26 | 31.52 | 46.17 |
| PE (%) | 0.7 | 1.92 | 0.55 | –15.40 (*) |

(∗) PE computed from the amplitude at the identified point force location

## 5. Real-world experiment

In this section, a real-world application is carried out on a simple structure in order to assess the identification ability of the GMR in operating conditions.

### *5.1. Description of the experimental set-up*

The structure under test is a steel parallelepiped box, excited on one of its faces by a shaker fed by a white noise signal and equipped with a force sensor (see Fig. 9). The dimensions and the thickness of the excited face are $(L_y, L_z) = (0.3 \text{ m}, 0.35 \text{ m})$ and $h = 5$ mm respectively, while the excitation point is approximately located at $(y_0, z_0) = (0.10 \text{ m}, 0.09 \text{ m})$.

As explained in section 3, the application of the GMR requires a measured vibration field $\mathbf{X}$ and a transfer function matrix $\mathbf{H}$ as input data. In the present experiment, the vibration field has been recorded by a scanning laser vibrometer on a grid of $(N_y \times N_z) = (19 \times 22)$ measurement points using the force sensor as phase reference. Furthermore, the measured velocity field

is, in the following, normalized to the signal delivered by the force sensor to obtain the vibration field resulting from the application of a unit point force (i.e. $F_p^{\text{ref}} = 1$). Regarding now the definition of the transfer functions matrix, it has been chosen to derive it from the FE model of a free plate having the same dimensions and material as the excited face, assuming that the measured bending motions are the only available data. Accordingly, the FE mesh of the equivalent plate has been built from the measurement grid and is made up with 378 shell elements [4].

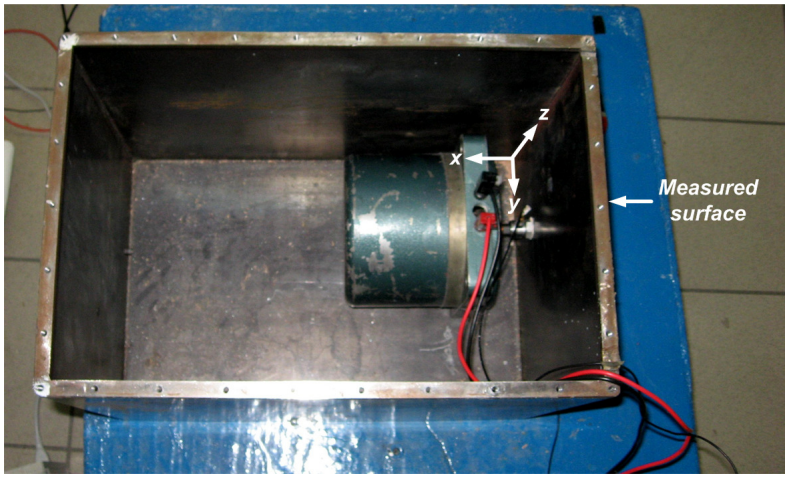


Figure 9: Experimental set-up - A parallelepiped box excited on one of its faces by a shaker

[4] In the present experimental validation, the FE mesh has been defined using 8 elements per bending wavelength. Consequently, the reconstruction mesh is theoretically valid up to 3 kHz.

*5.2. Application*

The analysis of the experimental set-up suggests the definition of two identification regions similar to those defined in the numerical application. More precisely, the first region, associated to the norm parameter $q_1$, contains the external point force only, while the second one, associated to the norm parameter $q_2$, corresponds to the boundaries of the excited face [see Fig. 10]. As explained in section 3.2, the values of the norm parameters must be chosen so as to reflect the spatial distribution of the forces to identify in the considered regions, i.e. the sparsity in the first region and the continuity of the boundary forces in the second region. Following the latter observation, the norm parameters $q_1$ and $q_2$ are respectively set to 0.5 and 2.

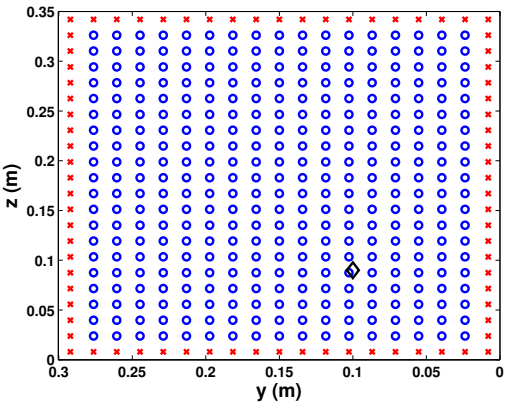


Figure 10: Definition of the identification regions - (○) region 1 (Point force), (×) region 2 (Boundary forces) and (◊) location of the point force

In the present experiment, the GMR is applied at 625 Hz. This specific frequency has been chosen because it is not a natural frequency of the sys-

tem[5]. In the following, because no reference excitation field is available, only the PE is evaluated from the results obtained for three values of the extra tuning parameter, corresponding respectively to the value used to initialize Algorithm 1 ($\mu_0$), that computed after the first iteration ($\mu_1$) and that reached at convergence ($\widehat{\mu}$) for a tolerance set to $10^{-3}$. Table 5 and Fig. 11 gather the results derived from the GMR.

Table 5: Peak error obtained at 625 Hz from the GMR

| **Indicator** | $\boldsymbol{\mu_0 = 1}$ | $\boldsymbol{\mu_1 = 3.66}$ | $\boldsymbol{\widehat{\mu} = 2.76 \times 10^{-9}}$ |
|---|---|---|---|
| PE (%) | –1.96 | 0.089 | -7.76 |

First of all, it is important to note that the least-squares solution is obtained by letting Algorithm 1 reach the convergence, which is obviously not the expected behavior. In the two other cases, the spatial distribution of the equivalent boundary forces are consistent with our expectations[6] and are somewhat equivalent whatever the value considered. On the contrary, the reconstruction of the excitation fields in the central region leads to noticeable differences. Indeed, Fig. 11 shows that the OMR (i.e. $\mu_0 = 1$) allows reasonably well quantifying and locating the external point force despite the presence of small reconstruction artifacts, since it is identified at

[5]At natural frequencies of a lightly damped structure, the mechanical response is driven by the modes of the system. This implies that the solution is generally not unique at these particular frequencies.

[6]Because a force-only model has been adopted here, the identified boundary forces are actually the sum of pure forces and equivalent forces due to the potential existence of boundary moments.

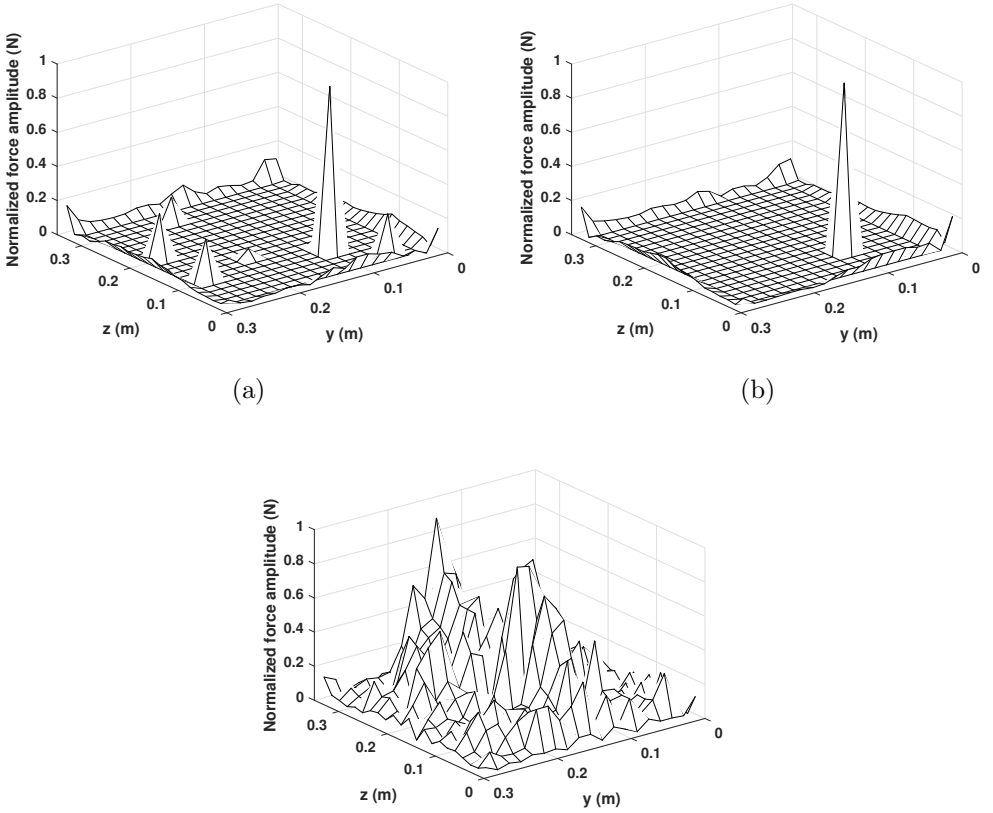


Figure 11: Reconstructed excitation field from the GMR at 625 Hz for (a) $\mu_0 = 1$, (b) $\mu_1 = 1.44$ and (c) $\widehat{\mu} = 2.76 \times 10^{-9}$

$(\widehat{y}_0, \widehat{z}_0) = (0.103\text{ m}, 0.088\text{ m})$ with a normalized amplitude $\widehat{F}_p$ of 0.98 (see Fig. 11a). Actually, the reconstruction artifacts, observed previously, are eliminated by applying the GMR for $\mu = \mu_1$, while leading to a better quantification of the point force amplitude (see Table 5 and Fig. 11b). These findings are in line with the conclusion drawn in section 3.2 and suggesting that completing the iterative process is not necessarily beneficial in terms of solution accuracy. More specifically, stopping the process right after the first iteration allows obtaining consistent solutions while limiting the computational cost of the iterative scheme described in Algorithm 1.

## 6. Conclusion

A generalized multiplicative regularization has been proposed for solving linear input estimation problems. The proposed method extends the ordinary multiplicative regularization by introducing an extra tuning parameter. In the course of this paper, the influence of this additional parameter according to the measurement noise level has been studied through a numerical experiment. It has been shown that the value of the extra tuning parameter tends to decrease as the noise level increases. However, because determining an optimal value of this parameter can be tricky, an original iterative procedure has been implemented. The application of this procedure both numerically and experimentally demonstrates the practical interest brought by the generalized multiplicative regularization in terms of solution accuracy and computational efficiency. More peculiarly, it has been shown that completing the iterative process is not necessarily beneficial in terms of solution accuracy and computational efficiency. Consequently, it is recommended to

stop the process right after the first iteration. The application of the proposed approach to other forms of regularization terms, such as mixed-norm regularization terms, will be the matter of future works.

## Appendix A. Application of the GMR for $\mu = 0.5$ and $\mu = 2$

We present in this section the results obtained from the GMR for two particular values of $\mu$, namely 0.5 and 2, for the numerical experiment carried out in section 3. These values have been chosen because they differently weight the relative importance of the data-fidelity and regularization terms and allows putting into perspective the results obtained from the OMR (i.e. $\mu = 1$).

### *Appendix A.1. GMR results for $\mu = 0.5$*

Table A.1 and Fig. A.1 summarize the results obtained from the GMR when $\mu = 0.5$. In particular, it is worth noting that the reconstructed excitation field is less accurate than that obtained from the OMR (i.e. $\mu = 1$) from weakly to highly noisy data. On the contrary, the opposite is observed for extremely noisy data, which is in agreement with the results presented in Figs. 4d and 8d. Actually, these conclusions are quite logical, since the data-fidelity term is promoted when $\mu > 1$. This is especially important for an SNR of 0 dB, since the information brought by the reconstruction model (see Eq. (4)) helps to obtain a physically consistent solution.

### *Appendix A.2. GMR results for $\mu = 2$*

Table A.2 and Fig. A.2 gather the results obtained from the GMR when $\mu = 2$. Contrary to what observes for $\mu = 0.5$, the excitation field identified is

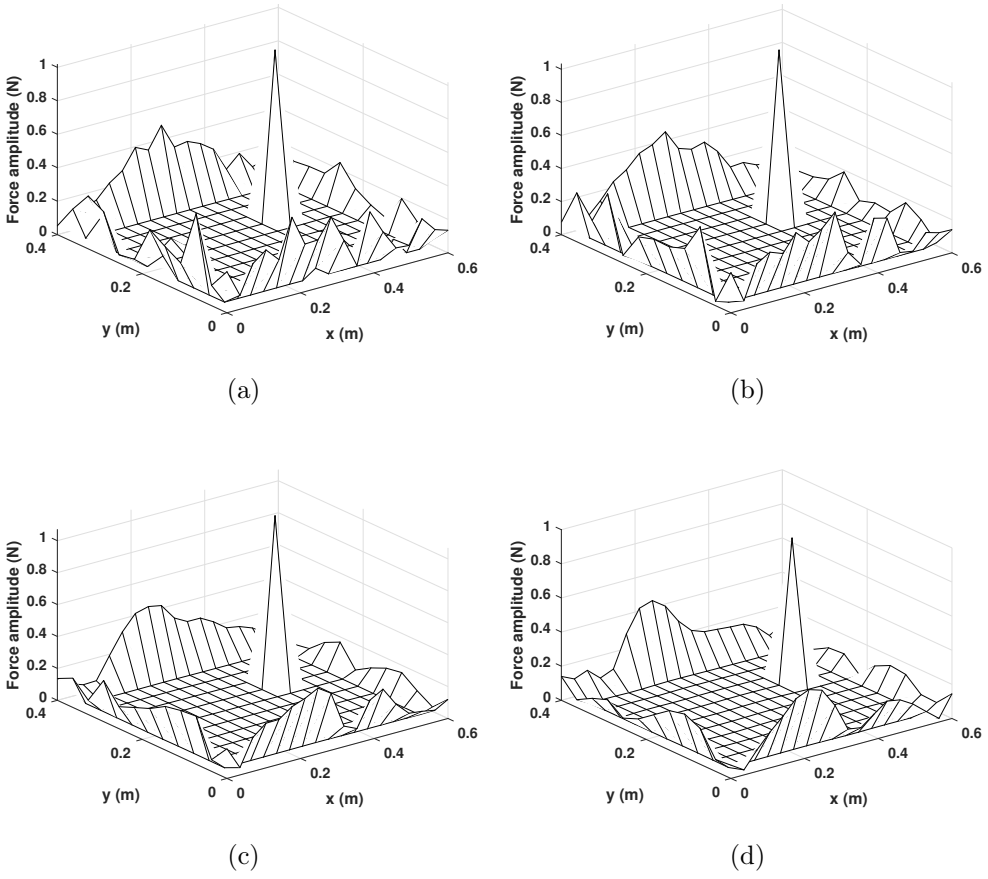


Figure A.1: Reconstructed excitation field at 350 Hz from the GMR for $\mu = 0.5$ – (a) SNR = 30 dB, (b) SNR = 20 dB, (c) SNR = 10 dB and (d) SNR = 0 dB

Table A.1: Performances of the GMR for $\mu = 0.5$ for various measurement noise levels – $N_{it}$: Number of iterations of the algorithm

| | **SNR** | | | |
|---|---|---|---|---|
| **Indicators** | **30 dB** | **20 dB** | **10 dB** | **0 dB** |
| GRE (%) | 56.66 | 48.58 | 45.62 | 63.82 |
| RERF (%) | 55.82 | 50.11 | 45.96 | 46.26 |
| PE (%) | 1.98 | 3.19 | 6.91 | –15.11 (*) |
| $N_{it}$ | 31 | 13 | 36 | 10 |

(∗) PE computed from the amplitude at the identified point force location

more accurate than that obtained for $\mu = 1$ for highly and moderately noisy data, which is in line with the results presented in sections 3.2 and 4.3. In the present case, the regularization term is favored, meaning that solutions based on prior knowledge of the sources to identify are promoted. This explains the disappointing results obtained for highly and extremely noisy data.

Table A.2: Performances of the GMR for $\mu = 2$ for various measurement noise levels – $N_{it}$: Number of iterations of the algorithm

| | **SNR** | | | |
|---|---|---|---|---|
| **Indicators** | **30 dB** | **20 dB** | **10 dB** | **0 dB** |
| GRE (%) | 22.84 | 21.33 | 25.46 | 76.30 |
| RERF (%) | 24.25 | 22.08 | 24.68 | 73.47 |
| PE (%) | 0.59 | 0.59 | –16.96 | –99.99 |
| $N_{it}$ | 12 | 13 | 16 | 24 |

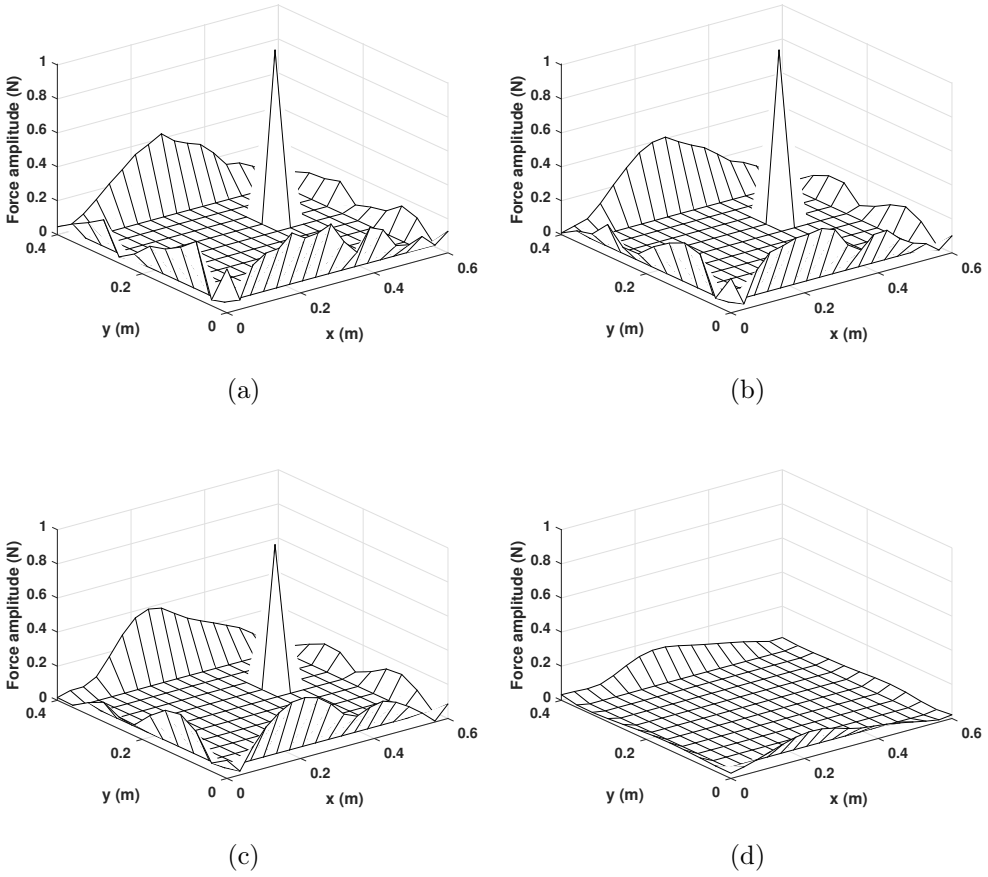


(a) (b)

(c) (d)

Figure A.2: Reconstructed excitation field at 350 Hz from the GMR for $\mu = 2$ – (a) SNR = 30 dB, (b) SNR = 20 dB, (c) SNR = 10 dB and (d) SNR = 0 dB

## References


[1] E. Lourens, E. Reynders, G. D. Roeck, G. Degrande, G. Lombaert, An augmented Kalman filter for force identification in structural dynamics, Mech. Syst. Signal Process. 27 (2012) 446–460.

[2] K. Maes, A. W. Smyth, G. D. Roeck, G. Lombaert, Joint input-state estimation in structural dynamics, Mech. Syst. Signal Process. 70–71 (2016) 445–466.

[3] W. Feng, Q. Li, Q. Lu, Force localization and reconstruction based on a novel sparse Kalman filter, Mech. Syst. Signal Process. 144 (2020) 106890 (28 pages).

[4] H. R. Busby, D. M. Trujillo, Optimal regularization of an inverse dynamics problem, Comput. Struct. 63 (2) (1997) 243–248.

[5] L. J. L. Nordström, A dynamic programming algorithm for input estimationon linear time-variant systems, Comput. Methods Appl. Mech. Engrg. 195 (2007) 6407–6427.

[6] A. Gonzàlez, C. Rowley, E. J. OBrien, A general solution to the identification of moving vehicle forces on a bridge, Int. J. Numer. Meth. Engng 75 (2008) 335–354.

[7] Y. Zhang, J. A. M. III, Examples of using structural intensity and the force distribution to study vibrating plates, J. Acoust. Soc. Am. 99 (1) (1996) 354–361.

[8] C. Pezerat, J.-L. Guyader, Force analysis technique: reconstruction of force distribution on plates, Acta Acust. United Ac. 86 (2) (2000) 322–332.

[9] M. S. Djamaa, Nouelaa, C. Pezerat, J.-L. Guyader, Mechanical Radial Force Identification of a Finite Cylindrical Shell by an Inverse Method, Acta Acust. United Ac. 92 (3) (2006) 398–405.

[10] A. Berry, O. Robin, F. Pierron, Identification of dynamic loading on a bending plate using the Virtual Fields Method, J. Sound Vib. 333 (26) (2014) 7151–7164.

[11] X. Xu, J. Ou, Force identification of dynamic systems using virtual work principle, J. Sound Vib. 337 (2015) 71–94.

[12] P. O'Donoughue, O. Robin, A. Berry, Time-resolved identification of mechanical loadings on plates using the virtual fields method and deflectometry measurements, Strain (2017) e12258 (14 pages).

[13] A. N. Tikhonov, Regularization of incorrectly posed problems, Soviet Math. 4 (1963) 1624–1627.

[14] A. N. Thite, D. J. Thompson, The quantification of structure-borne transmission paths by inverse methods. Part 2 : Use of regularization techniques, J. Sound Vib. 264 (2) (2003) 433–451.

[15] B. Qiao, X. Zhang, J. Gao, R. Liu, X. Chen, Sparse deconvolution for the large-scale ill-posed inverse problem of impact force reconstruction, Mech. Syst. Signal Process. 83 (2017) 93–115.

[16] C.-D. Pan, L. Yu, H.-L. Liu, Z.-P. Chen, W.-F. Luo, Moving force identification based on redundant concatenated dictionary and weighted $\ell_1$-norm regularization, Mech. Syst. Signal Process. 98 (2018) 32–49.

[17] G. H. Golub, M. Heath, G. Wahba, Generalized Cross-Validation as a method for choosing a good ridge parameter, Technometrics 21 (2) (1979) 215–223.

[18] P. C. Hansen, Rank-deficient and discrete ill-posed problems: numerical aspects of linear inversion, SIAM, Philadelphia, PA, USA, 1998.

[19] A. Pereira, J. Antoni, Q. Leclère, Empirical bayesian regularization of the inverse acoustic problem, Appl. Acoust. 97 (2015) 11–29.

[20] B. Efron, T. Hastie, I. Johnstone, R. Tibshirani, Least angle regression, Ann. Stat. 32 (2) (2004) 407–499.

[21] M. Aucejo, Structural source identification using a generalized Tikhonov regularization, J. Sound Vib. 333 (22) (2014) 5693–5707.

[22] A. Rezayat, V. Nassiri, B. D. Pauw, J. Ertveldt, S. Vanlanduit, Identification of dynamic forces using group-sparsity in frequency domain, Mech. Syst. Signal Process. 70–71 (2016) 756–768.

[23] M. Aucejo, O. D. Smet, A multiplicative regularization for force reconstruction, Mech. Syst. Signal Process. 85 (2017) 730–745.

[24] M. Aucejo, O. D. Smet, A space-frequency multiplicative regularization for force reconstruction problems, Mech. Syst. Signal Process. 104 (2018) 1–18.

[25] M. Aucejo, O. D. Smet, Multi-parameter multiplicative regularization: An application to force reconstruction problems, J. Sound Vib. 469 (2020) 115135 (15 pages).

[26] T. Le, R. Chartrand, T. J. Asaki, A variational approach to reconstructing images corrupted by poisson noise, J. Math. Imaging Vis. 27 (2007) 257–263.

[27] R. Tibshirani, Regression shrinkage and selection via the Lasso, J. R. Stat. Soc. Ser. B 58 (1) (1996) 267–288.

[28] T. Regińska, A regularization parameter in discrete ill-posed problems, SIAM J. Sci. Comput. 17 (3) (1996) 740–749.

[29] F. S. V. Bazán, Fixed-point iterations in determining the Tikhonov regularization parameter, Inverse Probl. 24 (2008) 035001 (15 pages).

[30] J. Antoni, A Bayesian approach to sound source reconstruction: optimal basis, regularization, and focusing, J. Acoust. Soc. Am. 131 (4) (2012) 2873–2890.

[31] M. Aucejo, O. D. Smet, An optimal bayesian regularization for force reconstruction problems, Mech. Syst. Signal Process. 126 (2019) 98–115.